Chinese Chemical Letters 33 (2022) 5208–5212

Contents lists available at ScienceDirect

Chinese Chemical Letters

journal homepage: www.elsevier.com/locate/cclet

Hydroxyl radical induced from hydrogen peroxide by cobalt manganese oxides for ciprofloxacin degradation

Shuandi Wang[a], Xiaodong Zhang[a], Guozhu Chen[a], Bao Liu[a], Hongmei Li[a], Junhua Hu[b], Junwei Fu[a,*], Min Liu[a,*]

[a] Hunan Joint International Research Center for Carbon Dioxide Resource Utilization, School of Physics and Electronics, State Key Laboratory of Powder Metallurgy, Hunan Provincial Key Laboratory of Chemical Power Sources, Central South University, Changsha 410083, China
[b] School of Materials Science and Engineering, Zhengzhou University, Zhengzhou 450002, China

ARTICLE INFO

Article history:
Received 30 September 2021
Revised 5 December 2021
Accepted 19 January 2022
Available online 25 January 2022

Keywords:
Catalytic decomposition
Hydrogen peroxide
Advanced oxidation processes
Ciprofloxacin
Pollutant degradation

ABSTRACT

Advanced oxidation processes (AOPs) are promising technology to remove organic pollutant in water. However, the main problem in the AOPs is the low generation of hydroxyl radical (•OH) owing to the low decomposition efficiency of hydrogen peroxide (H_2O_2). Herein, the spinel type cobalt acid manganese ($MnCo_2O_4$) with flower morphology was fabricated through a co-precipitation method. *In situ* Fourier transform infrared spectroscopy confirms that the $MnCo_2O_4$ with the optimal molar ratio of Co and Mn precursors (CM3, Co:Mn = 3) has more Lewis acid sites compared with single metal oxide catalysts (Co_3O_4 and Mn_2O_3), leading to the excellent performances for H_2O_2 decomposition rate constant on CM3, which is about 15.03 and 4.21 times higher than those of Co_3O_4 and Mn_2O_3, respectively. As a result, the obtained CM3 shows a higher ciprofloxacin degradation ratio than that of Co_3O_4 and Mn_2O_3. Furthermore, CM3 shows an excellent stability during several cycles. This work proposes effective catalysts for ciprofloxacin decomposition and provides feasible route for treating practical environmental problems.

Ciprofloxacin (CIP), with a total use of 5340 tons in China, has been considered as one of the most commonly used fluoroquinolones [1,2]. CIP has been detected in surface water, municipal wastewater, pharmaceutical wastewater and groundwater. These highest concentrations were 2500 μg/L, 14 mg/L, 31 mg/L and 14 μg/L, respectively [3–5]. The fluoroquinolones may have adverse effect on aquatic ecology by inducing the proliferation of bacterial resistance [6–9]. However, because high concentrations of organic pollutants are toxic to biochemical reactions, microorganisms and conventional physical and chemical treatments cannot effectively remove these pollutants [10,11]. Advanced oxidation processes (AOPs) with hydrogen peroxide (H_2O_2) are considered as a promising environmentally friendly strategy for the removal of organic pollutants [12–14]. AOPs can be effectively applied to organics degradation by improving the biodegradability or directly mineralizing of pollutants by oxidation, including Fenton/Fenton-like oxidation [15–18], ozonation [19–21], photocatalytic oxidation and peroxymonosulfate oxidation [22–25]. Among these technologies, the Fenton-like catalytic system is a promising choice for AOPs on account of the easy separation and recovery of solid catalyst, the wide working pH range and the high organic removal efficiency [26,27]. However, this system suffers from low content of free radicals and poor removal efficiency of organic pollutants, which is originated from slow decomposition of H_2O_2. This inspires us to design and develop efficient catalysts to produce more free radicals during AOPs.

H_2O_2 is a Lewis base that is readily absorbed by the Lewis acid sites and produces a large number of •OH [28]. However, catalytic performance of single metal oxide is limited by the insufficient Lewis acid sites and the slow redox cycles of metal valence [29,30]. In order to produce more oxygen-containing free radicals, previous studies reported that doping MnO_x with other metal to form mixed metal oxides tended to produce more oxygen-containing free radicals [26]. For examples, the chemical states and properties of Mn can be substantially tuned in the perovskite- and spinel-type oxides [31–34]. Composite metal oxides possess the sufficient Lewis acid sites and fast redox cycles of metal valence due to the interactions between different metal atoms [35–37]. Mi *et al.* have investigated the electron communication between the different metal sites in composite metal oxides [38]. The result indicated that the composite metal oxides have synergistic effect Co and Mn sites, which is beneficial for generating •OH abundantly. Therefore,

* Corresponding authors.
E-mail addresses: fujunwei@csu.edu.cn (J. Fu), minliu@csu.edu.cn (M. Liu).

https://doi.org/10.1016/j.cclet.2022.01.055
1001-8417/

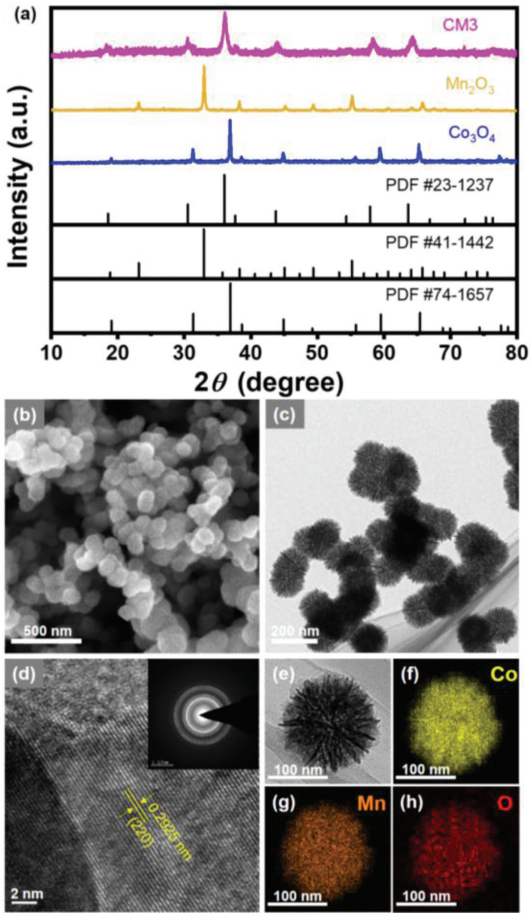

Fig. 1. (a) XRD patterns of CM3, Mn_2O_3, Co_3O_4 candidates. (b) SEM and (c) TEM images of CM3. (d) HRTEM and SAED pattern (inset) images of CM3 with submicron-sized particles. (f-h) Elemental mapping of Mn, Co and O for CM3 (e).

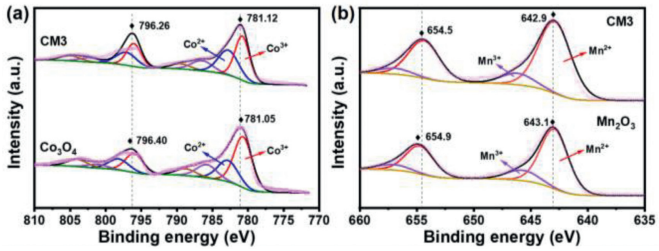

Fig. 2. XPS spectra of CM3, Co_3O_4 and Mn_2O_3: (a) Co 2p, (b) Mn 2p.

we considered that composite metal oxides can greatly improve the catalytic oxidation efficiency.

In this study, the spinel $MnCo_2O_4$ (CM3) has been synthesized through a facile co-precipitation method. X-ray diffraction spectroscopy (XRD), scanning electron microscopy (SEM) and transmission electron microscopy (TEM) were carried out to verify its crystal structure and morphology. The performance test results show that the spinel CM3 possesses excellent performance in the decomposition of H_2O_2 due to the synergistic effect of Co and Mn. The rate constant of H_2O_2 degradation rate constant for CM3 was about 15.03 and 4.21 times higher than those of Co_3O_4 and Mn_2O_3, respectively. Meanwhile, as the typical organic quinolones, CIP was selected for the target organic pollutant to evaluate the efficiency of AOPs among catalysts. Compared with single metal oxides, spinel CM3 can remarkably reduce the energy barrier of producing $^{\bullet}OH$. Therefore, CM3/H_2O_2 system shows great degradation ratio of CIP (10 mg/L), which reach up to 81% in 100 min, and it is higher than that of Co_3O_4 and Mn_2O_3. The experimental results and density functional theory (DFT) calculations reveal the synergistic effect of Co and Mn in CM3 for outstanding catalytic performance. Thus, the CM3 shows outstanding catalytic performance and provides feasible way for treating practical environmental problems.

The crystal structure of the synthesized samples was analyzed by XRD (Fig. 1a) [39–41]. The crystal structure of control samples is consistent with the standard sample, which can be correspond to the cubic Mn_2O_3 (PDF #41–1442) and cubic spinel Co_3O_4 (PDF #74–1657), respectively. Among the binary transition metal oxide, the obtained CM3 agrees well with the standard spinel $MnCo_2O_4$ (PDF #23–1237), indicating the successful synthesis of single-phase cubic spinel.

To characterize the morphology and structure of catalysts, SEM and TEM were carried out (Figs. 1b-h). Clearly, the CM3 has a diameter of about 150 nm with well nanoflower-like structures and assembled by nanosheets (Fig. 1b). The CM3 shows high specific surface area of 111.4 m^2/g (Table S1 and Fig. S1 in Supporting information), favoring for the heterogeneous catalytic reaction. On the contrary, the prepared Mn_2O_3 and Co_3O_4 show a morphology of nanoparticle (Fig. S2 in Supporting information).

TEM image confirms the nanoflower-like structure which is assembled by nanosheets (Fig. 1c). The high-resolution transmission electron microscopy (HRTEM) image and the selected area electron diffraction (SAED) of CM3 are shown in Fig. 1d. The inter-planar distance measured in HRTEM image was measured to be 2.9 Å, which matches well to the (220) planes of the spinel $MnCo_2O_4$ (Fig. 1d). The SAED pattern exhibits concentric rings composed of bright discrete diffraction spots of CM3, indicating that the polycrystalline nature for CM3. The diffraction rings are indexed to (111), (220), (311), (400), (511), and (440) planes of XRD patterns in $MnCo_2O_4$ structure [42]. The investigation based on energy dispersive X-ray spectroscopy (Figs. 1e-h) reveals a uniform distribution of Mn, Co and O in the CM3 nanoflower-like structure.

In order to identify the oxidation state of Co and Mn in the CM3, Co_3O_4 and Mn_2O_3, the X-ray photoelectron spectroscopy (XPS) of the Co and Mn 2p were recorded and fitted as Fig. 2 [43]. For the Co_3O_4 (Fig. 2a), two main peaks of Co $2p_{3/2}$ and Co $2p_{1/2}$ are located at 781.05 and 796.40 eV, respectively [44]. For the CM3 (Fig. 2a), these two main peaks are located at 781.12 and 796.26 eV, which indicates co-exist of Co^{2+} and Co^{3+} species in the Co_3O_4 and CM3 [45]. For the Mn_2O_3 (Fig. 2b), two main peaks are located at 643.1 and 654.9 eV, respectively [46]. For the CM3 (Fig. 2b), these two main peaks shift to 642.9 and 654.5 eV, demonstrating that introducing Co can well adjust the valence state of Mn [47].

The catalytic degradation experiments were conducted to evaluate the catalytic performances of different catalysts. The concentration of H_2O_2 was determined by titanium potassium oxalate method (Fig. S3 in Supporting information) [48,49]. As shown in Fig. 3a, within 15 min, the H_2O_2 degradation efficiencies for Mn_2O_3 and Co_3O_4 are about 40% and 20%, respectively. Notably, the H_2O_2 degradation efficiency for CM3 is up to 99%. The rate constant (k) was then evaluated based on linear fitting between $-\ln(C/C_0)$ and time t [50,51]. As shown in Fig. 3b, the H_2O_2 degradation rate constant in the CM3 (0.284 min^{-1}) was about 15.03 and 4.21 times higher than those of Co_3O_4 (0.0189 min^{-1}) and Mn_2O_3 (0.0675 min^{-1}), confirming the high performance of CM3. Furthermore, the catalytic activity did not decrease obviously, indicating its good stability and long lifetime (Fig. S4 in Supporting information).

The catalytic performances of the as-prepared oxides for wastewater treatment were further compared. CIP, as a typical industrial pollutant, is chosen as a model to examine the degradation

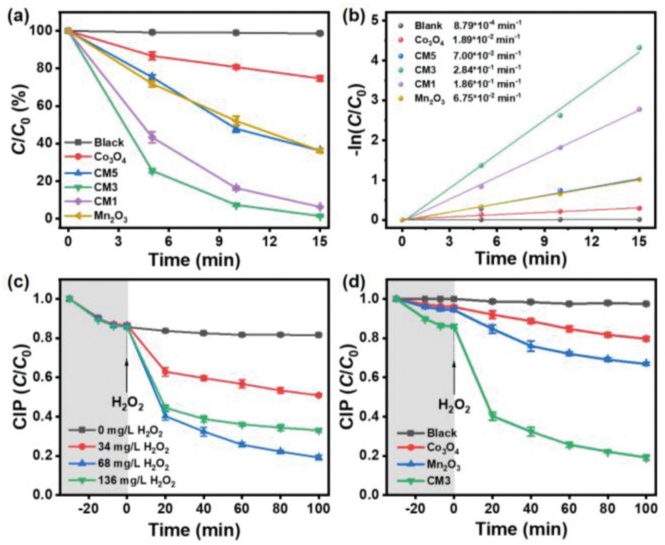

Fig. 3. (a) H_2O_2 degradation in the different catalyst systems. Conditions: $[H_2O_2]_{ini} = 30$ mmol/L, catalyst = 0.05 g/L in 100 mL reaction solution. (b) The fitted plots of $-\ln(C/C_0)$ with the reaction time in H_2O_2 degradation. (c) Effects of H_2O_2 dosage on CIP degradation in CM3 catalyst system. Conditions: catalyst = 0.2 g/L, $[CIP]_{ini} = 10$ mg/L in 100 mL reaction solution. (d) CIP degradation in the different catalyst systems. Conditions: $[CIP]_{ini} = 10$ mg/L, $[H_2O_2]_{ini} = 68$ mg/L and catalyst = 0.2 g/L in 100 mL reaction solution.

efficiency of organic pollutants by the as-prepared oxides. The effects of catalyst dosage and temperature on CIP degradation were studied (Figs. S5 and S6 in Supporting information). The influence of H_2O_2 dosage on the performance of CM3 is shown in Fig. 3c. The results showed that degradation efficiency of CIP increased to 81% with the dosage of H_2O_2 increasing from 0 mg/L to 68 mg/L. While a further increase of H_2O_2 dosage (from 68 mg/L to 136 mg/L) hindered the degradation of ciprofloxacin (decreased from 81% to 64%). The reason can be attributed to that the residual H_2O_2 can act as a sacrificial agent for free radicals (•OH) [52]. These results showed that the optimal H_2O_2 concentration was 68 mg/L. Under the optimal H_2O_2 dosage, the binary transition metal oxides CM3 (81%) have excellent CIP degradation performance compared with single metal oxides Co_3O_4 (22%) and Mn_2O_3 (34%) in Fig. 3d. The initial rate constants of CM3, Mn_2O_3 and Co_3O_4 catalyst systems are 0.11 min^{-1}, 0.023 min^{-1} and 0.01 min^{-1}, respectively (Fig. S7 and Table S2 in Supporting information) [53,54]. And the CM3 Fenton-like system can improve the TOC removal rate of CIP from 10.23% and 22.6% to 50.33% comparing to the Co_3O_4 and Mn_2O_3, respectively (Figs. S8 and S9 in Supporting information) [55].

In order to explore which free radicals involved the CIP degradation, *p*-benzoquinone (BQ) and *t*-butanol (TBA) were added to the reaction solution to detect the reactive radicals [16,56]. Fig. 4a shows that the degradation of CIP was greatly inhibited by adding 50 mmol/L BQ or 50 mmol/L TBA, indicating that both $O_2^{\bullet-}$ and •OH promoted the degradation of CIP. Apparently, significant inhibiting effect was observed in the presence of 50 mmol/L TBA, implying that •OH radicals play the most important role in CIP degradation. In order to reveal the reaction mechanism of the CIP degradation, we detect free radical species by oxidation current, free radical quenching, 5,5-dimethylpyrroline-1-oxide (DMPO) trapped electron paramagnetic resonance (EPR) technique and photoluminescence spectra of benzoic acid mixed [57,58]. In the chronoamperometry curves, it can be observed that the oxidation current in H_2O_2 solution increases after adding CM3. While the change before and after adding CM3 in blank solution is negligible (Fig. 4b). This indicates that some species are produced in the interaction between CM3 and H_2O_2. Due to its high reducibility, the most likely increase in oxidation current is •OOH, which is more reducible than H_2O_2. In addition, we detected the •OH in different catalyst systems with DMPO trapped EPR technique [59]. As shown in Fig. 4c, there are more •OH in CM3-H_2O_2 system. We detected •OH in different systems by photoluminescence [16]. The CM3 has a high fluorescence intensity from the photoluminescence spectra (Fig. 4d). The H_2O_2 decomposition efficiency can be obviously increased in the CM3 Fenton-like reaction. Usually, benzoic acid (BA) was used as a probe molecule to detect concentration of •OH [60]. In subsequent experiments, 2 mmol/L BA was selected as the initial probe concentration. The generation of radicals in the different systems is shown in Fig. 4e. Compared with single metal oxides Co_3O_4 and Mn_2O_3, the addition of the CM3 greatly increased •OH generation. These results demonstrated that CM3 could facilitate the production of more •OH due to the improved decomposition efficiency of H_2O_2, which leads to the efficient degradation of CIP in CM3-H_2O_2 system.

To explore the surface acid sites on CM3, the distribution of Brønsted (B) and Lewis (L) acidity were measured by *in-situ* diffuse-reflectance infrared Fourier-transform (DRIFT) spectra with pyridine using pyridine as a probe (Fig. 4f). Because H_2O_2 is a Lewis base that is readily absorbed by the Lewis acid sites and produces a large number of •OH [28]. The band at 1550–1640 cm^{-1} and 1450 cm^{-1} are assigned to found for pyridine absorbed at L acid sites while the 1540 cm^{-1} band is absorption intensity at B acid sites [61]. The experimental results show that CM3 exhibited much stronger signal intensity, which indicates that the L acid sites in CM3 are far more than other comparison samples. Note that H_2O_2 was a L base, the enhanced adsorption of H_2O_2 onto these CM3 should contribute to the activation of H_2O_2 for CIP oxidation. Compared with Co_3O_4 and Mn_2O_3, the formation of L acid sites indicating the presence of synergistic effect between the Co and Mn sites. In addition, the voltammetric integral area of the cyclic voltammetry (CV) was another parameter to reflect the redox-active sites of the catalysts (Fig. S10 in Supporting information) [45,62]. CM3 has a large voltammetric integral areas. Indicating the bimetallic oxides has more redox-active sites, which is beneficial for catalytic reactions. This is consistent with the results of *in-situ* DRIFT spectra.

From the above analyses, it can be concluded that the freely diffusible •OH formed by the catalyst is the main active substance in the oxidation reaction of the pollutant. In order to understand the synergy between Mn and Co, DFT calculations were performed to compare catalytic activity of Co_3O_4, Mn_2O_3 and CM3 systems [63]. Fig. 5 illustrated the free energy change of H_2O_2 decomposition into •OH by the cleavage of O–O bonds on CM3, Co_3O_4 and Mn_2O_3 surface, respectively. The free energy differences of •OH generation on Co_3O_4, Mn_2O_3 and CM3 were 2.35, 2.55 and 3.95 eV, respectively. Compared with Co_3O_4 and Mn_2O_3, CM3 is more conducive to activation of H_2O_2 to produce •OH. The adsorption of H_2O_2 and the desorption of •OH were calculated (Fig. S11, Tables S3 and S4 in Supporting information). From the adsorption energy of H_2O_2, the adsorption energy of $MnCo_2O_4$ (CM3) is more negative, and the O–O bond almost breaks during the adsorption. This indicates that $MnCo_2O_4$ (CM3) has excellent ability to activate H_2O_2. From the perspective of •OH desorption energy, Mn_2O_3 has a lower desorption energy, but a higher dissociation energy, which affects its catalytic performance. Moreover, the surface •OH of $MnCo_2O_4$ (CM3) has moderate desorption energy. In general, $MnCo_2O_4$ (CM3) is more capable of activating H_2O_2 and generating •OH to degrade CIP.

In this study, the spinel type CM3 with significant H_2O_2 decomposition efficiency was fabricated through a co-precipitation method. CM3 has more L acid sites due to the synergistic effect of Co and Mn. Compared with Co_3O_4 and Mn_2O_3, CM3 plays a significant role on the decomposition of H_2O_2 in a Fenton-like sys-

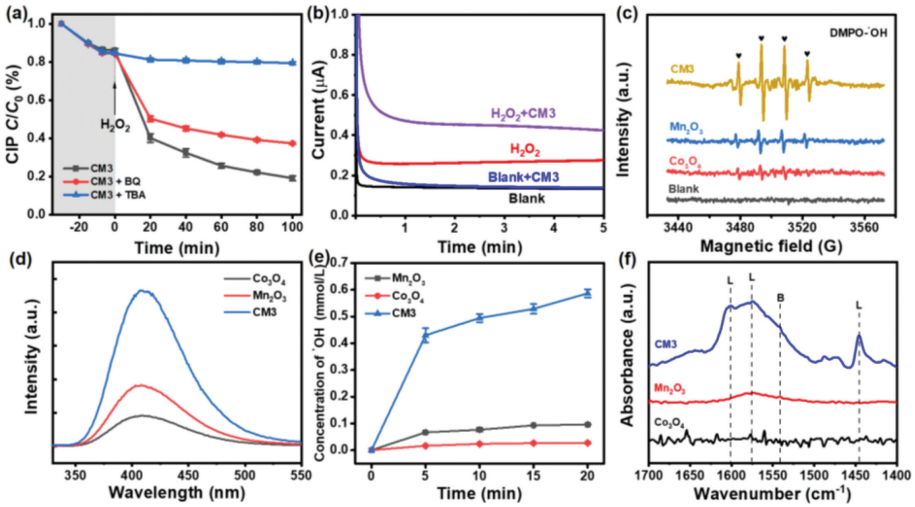

Fig. 4. (a) Inhibiting effects of different radical scavengers on degradation of CIP by CM3. Conditions: $[CIP]_{ini} = 10$ mg/L, [BQ] = 50 mmol/L, [TBA] = 50 mmol/L, catalyst = 0.2 g/L and $[H_2O_2]_{ini} = 68$ mg/L in 100 mL reaction solution. (b) Chronoamperometry curves in blank solution, blank solution with CM3, H_2O_2 solution, and H_2O_2 solution with CM3. Tests were made in 50 mmol/L Na_2SO_4 electrolyte at a scanning rate of 20 mV/s. (c) DMPO spin trapping EPR spectra of ·OH. (d) Photoluminescence spectra of benzoic acid mixed with different solutions for the Fenton-like reaction within 100 min. Conditions: $[CIP]_{ini} = 10$ mg/L, [BA] = 2 mmol/L, catalyst = 0.2 g/L and $[H_2O_2]_{ini} = 68$ mg/L in 100 mL reaction solution. (e) The generation of radicals in different systems. Conditions: $[CIP]_{ini} = 10$ mg/L, [BA] = 2 mmol/L, catalyst = 0.2 g/L and $[H_2O_2]_{ini} = 68$ mg/L in 100 mL reaction solution. (f) *In-situ* DRIFTS spectra of catalysts with pyridine as probe at 25 °C.

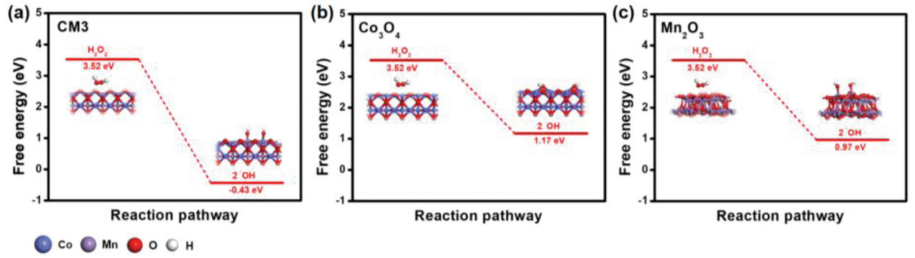

Fig. 5. Free energy diagrams for the H_2O_2 decomposition into ·OH on surface of CM3 (a), Co_3O_4 (b) and Mn_2O_3 (c), respectively.

tem. The rate constant of H_2O_2 degradation rate constant by CM3 was about 15.03 and 4.21 times higher than that by pure Co_3O_4 and Mn_2O_3, respectively. Accordingly, the CM3/H_2O_2 system shows great degradation ratio of CIP (10 mg/L), and reaches up to 81% in 100 min, which is higher than that of Co_3O_4 and Mn_2O_3. Meanwhile, the CM3 shows favorable stability for several cycles. DFT calculations further elucidate the dissociation of H_2O_2. This work provides a new way to design efficient, stable and harmless Fenton-like catalysts and achieve excellent environmental remediation effect.

Declaration of competing interest

The authors declare no conflict of interest.

Acknowledgments

The authors gratefully thank the International Science and Technology Cooperation Program (Nos. 2017YFE0127800 and 2018YFE0203400), National Natural Science Foundation of China (Nos. 21872174, 22002189 and U1932148), Hunan Provincial Science and Technology Program (Nos. 2017XK2026 and 2017TP1001), Hunan Provincial Natural Science Foundation (Nos. 2020JJ2041, 2020JJ5691 and 2021JJ30864), Key R&D Program of Hunan Province (No. 2020WK2002), Shenzhen Science and Technology Innovation Project (No. JCYJ20180307151313532).

Supplementary materials

Supplementary material associated with this article can be found, in the online version, at doi:10.1016/j.cclet.2022.01.055.

References

[1] Q.Q. Zhang, G.G. Ying, C.G. Pan, Y.S. Liu, J.L. Zhao, Environ. Sci. Technol. 49 (2015) 6772–6782.
[2] Z. Cai, A.D. Dwivedi, W.N. Lee, et al., Environ. Sci.: Nano 5 (2018) 27.
[3] J. Duan, H. Ji, T. Xu, et al., Chem. Eng. J. 406 (2021) 126752.
[4] J. Ma, L. Chen, Y. Liu, et al., J. Hazard. Mater. 418 (2021) 126180.
[5] S. Li, T. Huang, P. Du, W. Liu, J. Hu, Water Res. 185 (2020) 116286.
[6] J. Yang, J.J. Pignatello, B. Pan, B. Xing, Environ. Sci. Technol. 51 (2017) 8972–8980.
[7] U. Jans, C. Prasse, U. von Gunten, Environ. Sci. Technol. 55 (2021) 3313–3321.
[8] Y. Wang, C. Zhou, J. Wu, J. Niu, Chin. Chem. Lett. 31 (2020) 2673–2677.
[9] Y. Zhou, Y. Gao, S.Y. Pang, et al., Water Res. 145 (2018) 210–219.
[10] Y. Zhang, C. Liu, B. Xu, F. Qi, W. Chu, Appl. Catal. B 199 (2016) 447–457.
[11] L. Ling, Y. Liu, D. Pan, et al., Chem. Eng. J. 381 (2020) 122607.
[12] X. Yang, X. Cheng, A.A. Elzatahry, et al., Chin. Chem. Lett. 30 (2019) 324–330.
[13] S. Chen, T. Luo, K. Chen, et al., Angew. Chem. Int. Ed. 60 (2021) 16607–16614.
[14] J. Zheng, D. Song, H. Chen, et al., Chin. Chem. Lett. 31 (2020) 1109–1113.
[15] J. Zhan, M. Li, X. Zhang, et al., Chin. Chem. Lett. 31 (2020) 715–720.
[16] B. Shen, C. Dong, J. Ji, M. Xing, J. Zhang, Chin. Chem. Lett. 30 (2019) 2205–2210.
[17] C. Guo, D. Yue, S. Wang, X. Qian, Y. Zhao, Chin. Chem. Lett. 31 (2020) 1978–1981.
[18] Z. Wang, M. Liu, F. Xiao, et al., Chin. Chem. Lett. 33 (2022) 653–662.
[19] Z. Guo, Y. Xie, J. Xiao, et al., J. Am. Chem. Soc. 141 (2019) 12005–12010.
[20] S. Afzal, X. Quan, J. Zhang, Appl. Catal. B 206 (2017) 692–703.
[21] Y. Ding, J. Wang, S. Xu, K.Y.A. Lin, S. Tong, Sep. Purif. Technol. 207 (2018) 92–98.
[22] Y. Lee, D. Gerrity, M. Lee, et al., Environ. Sci. Technol. 50 (2016) 3809–3819.
[23] Y. Yao, Y. Cai, G. Wu, et al., J. Hazard. Mater. 296 (2015) 128–137.
[24] X. Ao, W. Liu, Chem. Eng. J. 313 (2017) 629–637.
[25] M. Du, Q. Yi, J. Ji, et al., Chin. Chem. Lett. 31 (2020) 2803–2808.

[26] S. Zhu, S.H. Ho, C. Jin, X. Duan, S. Wang, Environ. Sci.: Nano 7 (2020) 368–396.
[27] X. Yan, Y. Song, X. Wu, et al., Nanoscale 9 (2017) 2317–2323.
[28] H. Liang, R. Liu, X. An, et al., Chem. Eng. J. 414 (2021) 128669.
[29] H. Li, J. Shang, Z. Yang, et al., Environ. Sci. Technol. 51 (2017) 5685–5694.
[30] M. Liu, Z. Feng, X. Luan, et al., Environ. Sci. Technol. 55 (2021) 6042–6051.
[31] X. Qi, H. Tian, X. Dang, et al., Anal. Methods 11 (2019) 1111–1124.
[32] J.T. Mefford, W.G. Hardin, S. Dai, K.P. Johnston, K.J. Stevenson, Nat. Mater. 13 (2014) 726–732.
[33] C. Li, X. Han, F. Cheng, et al., Nat. Commun. 6 (2015) 7345.
[34] L. Luo, Y. Zhang, F. Li, et al., Anal. Chim. Acta 788 (2013) 46–51.
[35] M. Li, Y. Xiong, X. Liu, et al., Nanoscale 7 (2015) 8920–8930.
[36] S. Saha, S.B Abd Hamid, RSC Adv. 6 (2016) 96314–96326.
[37] H. Li, K. Liu, J. Fu, et al., Nano Energy 82 (2021) 105767.
[38] X. Mi, Y. Li, X. Ning, et al., Chem. Eng. J. 358 (2019) 299–309.
[39] K. Chen, H. Li, Y. Xu, et al., Nanoscale 11 (2019) 5967–5973.
[40] J. Fu, L. Zhu, K. Jiang, et al., Chem. Eng. J. 415 (2021) 128982.
[41] K. Chen, K. Liu, P. An, et al., Nat. Commun. 11 (2020) 4173.
[42] R. Yuan, H. Li, X.A. Zhang, et al., J. Energy Storage 29 (2020) 101300.
[43] J. Fu, K. Liu, K. Jiang, et al., Adv. Sci. 6 (2019) 1900796.
[44] X. Xie, C. Ni, Z. Lin, et al., Chem. Eng. J. 396 (2020) 125205.
[45] L. Pi, N. Yang, W. Han, et al., Chem. Eng. J. 334 (2018) 1297–1308.
[46] K. Lei, X. Han, Y. Hu, et al., Chem. Commun. 51 (2015) 11599–11602.
[47] K. Cheng, F. Yang, G. Wang, J. Yin, D. Cao, J. Mater. Chem. A 1 (2013) 1669–1676.
[48] Z. Wang, B. Song, J. Li, X. Teng, Chemosphere 270 (2021) 128652.
[49] Y. Zhang, X. Xu, J. Cai, Y. Pan, M. Zhou, Chemosphere 266 (2021) 129063.
[50] C. Ma, S. Feng, J. Zhou, et al., Appl. Catal. B 259 (2019) 118015.
[51] Y. Qin, Y. Sun, Y. Li, et al., Chin. Chem. Lett. 31 (2020) 774–778.
[52] P. Thanekar, P.R. Gogate, Sep. Purif. Technol. 239 (2020) 116563.
[53] J. Duan, H. Ji, X. Zhao, et al., Chem. Eng. J. 393 (2020) 124692.
[54] J. Duan, H. Ji, W. Liu, et al., Chem. Eng. J. 359 (2019) 1617–1628.
[55] H. Liang, R. Liu, C. Hu, et al., J. Hazard. Mater. 406 (2021) 0304–3894.
[56] M. Yu, H. Liang, R. Zhan, L. Xu, J. Niu, Chin. Chem. Lett. 32 (2021) 2155–2158.
[57] F. Yang, X. Chu, J. Sun, et al., Chin. Chem. Lett. 31 (2020) 2784–2788.
[58] Q. Yang, Z. Feng, M. Liu, et al., Chin. Chem. Lett. 32 (2021) 3393–3397.
[59] C. Dong, J. Ji, B. Shen, M. Xing, J. Zhang, Environ. Sci. Technol. 52 (2018) 11297–11308.
[60] N. Yan, F. Liu, Q. Xue, et al., Chem. Eng. J. 274 (2015) 61–68.
[61] H. Zhang, W. Yang, I.I. Roslan, S. Jaenicke, G.K. Chuah, J. Catal. 375 (2019) 56–67.
[62] A.N. Naveen, S. Selladurai, Electrochim. Acta 125 (2014) 404–414.
[63] Y. Lin, K. Liu, K. Chen, et al., ACS Catal. 11 (2021) 6304–6315.